THE ASTROPHYSICAL JOURNAL, 369:L21–L25, 1991 March 10

THE IMAGING PERFORMANCE OF THE *HUBBLE SPACE TELESCOPE*

CHRISTOPHER J. BURROWS,[1,2] JON A. HOLTZMAN,[3,4] S. M. FABER,[3,5] PIERRE Y. BELY,[1,2]
HASHIMA HASAN,[1] C. R. LYNDS,[3,6] AND DANIEL SCHROEDER[7]

Received 1990 October 17; accepted 1990 December 7

ABSTRACT

The *Hubble Space Telescope* suffers from significant spherical aberration and does not give the predicted diffraction-limited images. A maximum of about 16% of the light from a point source is concentrated in a 0".1 radius, where 70% was expected. The images consist of this core, surrounded by a complex 4".0 diameter inner halo that contains most of the light and is caused by portions of the primary mirror that are not focusing correctly. Ground test results uncovered by the Allen Commission agree with results derived from studies of the on-orbit imagery.

The pointing performance is also degraded, with guide stars for fine lock presently limited to 13.5 mag, compared to an expected limit of 14.5 mag. Some areas of the sky are therefore not accessible in fine lock. In addition, the spacecraft undergoes severe pointing disturbances during portions of the orbit, caused by thermal shocks.

Nevertheless, *HST* represents a unique resource for high-resolution imaging of low-contrast bright objects through deconvolution techniques. Such techniques rely on the detailed information about the PSF that is given here. *HST* can split higher contrast fields into components when photometric accuracy is not important. There is a loss of about 2 mag in limiting magnitude for point sources.

Subject headings: analytical methods — image processing — instruments — numerical methods — photometry — sky photographs — ultraviolet: general

1. INTRODUCTION

The *Hubble Space Telescope* (*HST*) was launched on 1990 April 24. The spacecraft has performed well in most respects but is seriously compromised in imaging and pointing performance when compared to specifications.

HST contains a 2.4 m aperture f/24 Ritchey-Chrétien telescope capable of imaging from 115 nm out to the thermal infrared. It carries a complement of five scientific instruments (SIs), together with three interferometric fine guidance sensors (FGSs), that simultaneously view a 28′ diameter field. A summary of the expected capabilities of the observatory and its scientific potential is given in Hall (1982).

Optical tests on the observatory and examination of ground tests and equipment used in the primary mirror fabrication have clearly demonstrated that *HST* suffers from spherical aberration. Light striking near the edge of the primary mirror is brought to a focus about 40 mm behind the focus of light passing close to the secondary baffle. The result is that no choice of focal plane yields the expected diffraction limited images. The top level specification was that 70% of the energy be focused in a 0".1 radius, but the present, and close to optimum, focus setting gives only about 16%. The optical results are outlined in the next section.

Image quality is also critically dependent on the performance of the pointing control system. The spacecraft undergoes two periods of large-amplitude pointing excursions per orbit, associated with sunrise and sunset, and apparently random lower amplitude disturbances. During quiescent periods, the spacecraft achieves a stability of about 0".007 rms, but this falls short of the specification which required that such performance be maintained for 24 hr. Further, the FGSs are not guiding well on faint stars, perhaps an indirect result of the spherical aberration. Consequently, there is a loss of sky coverage at high Galactic latitude, especially for the Wide-Field/Planetary Camera (WFPC). The pointing performance is discussed in § 3.

A general outline of the effects of the degraded performance on the scientific program and our conclusions are given in § 4.

2. INSTANTANEOUS IMAGING PERFORMANCE

The Optical Telescope Assembly (OTA) contains a 2.4 m diameter f/2.3 hyperbolic primary mirror, separated from the hyperbolic secondary by 4.9 m (Schroeder 1987; Burrows 1990). In the design, the conic constants on the primary and secondary mirrors are chosen to yield zero third-order spherical aberration and field coma.

The secondary mirror can be precisely positioned with 6 degrees of rigid-body freedom to collimate the telescope. Three radial shearing interferometers called wavefront sensors are located at the inner edges of the FGS fields of view. They were designed to measure the wavefront and allow accurate collimation, but their performance is degraded by the spherical abberation. As a result most of the diagnosis, focusing, and collimation efforts had to rely on analysis of the imagery from the SIs. Behind the primary mirror are 24 force actuators arranged in two concentric circles. They can be used to make small adjustments to the mirror figure but do not have sufficient dynamic range to correct the spherical aberration.

[1] Space Telescope Science Institute; operated by the Association of Universities for Research in Astronomy, Inc. under contract with the National Aeronautics and Space Administration. Postal address: 3700 San Martin Drive, Baltimore, MD 21218.
[2] Also Astrophysics Division, Space Science Department of ESA.
[3] Wide-Field/Planetary Camera Investigation Definition Team.
[4] Lowell Observatory, Mars Hill Road, Flagstaff, AZ 86001.
[5] UCO/Lick Observatories, Board of Studies in Astronomy and Astrophysics, University of California, Santa Cruz, Santa Cruz, CA 95064.
[6] NOAO, P.O. Box 26732, Tucson, AZ 85726.
[7] Department of Physics and Astronomy, Beloit College, Beloit, WI 53511.

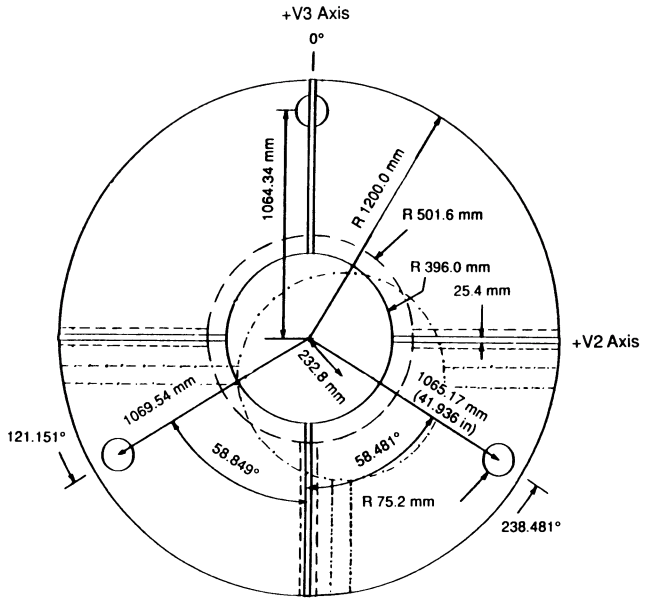

FIG. 1.—The nominal exit pupil used in the models. Solid lines define the obscurations in the OTA consisting of the secondary mirror baffle, spider supports, the primary mirror pads, and outer mask. Dashed lines define the extra obscurations introduced by the Cassegrain obscuration and spider supports at the center of PC chip 5 for a properly centered beam. The dotted lines show their positions on the OTA axis (at the corner of the chip). The FOC f/96 and f/48 modes do not introduce any extra pupil obscurations.

The primary mirror is supported by three 15 cm diameter circular pads that mask corresponding areas in the pupil. The secondary mirror assembly is mounted on a conventional four-legged spider mount, which causes a cross-shaped obscuration of the incoming light. The central third of the beam is obscured by the secondary mirror baffle. The OTA entrance pupil is therefore defined by a mask at the edge of the primary mirror, the secondary mirror spiders, the primary mirror pads, and the secondary baffle, as illustrated in Figure 1.

The WFPC (Griffiths 1990) reimages the OTA focal plane, where a four-faceted pyramid can be rotated to divide the field into one of two possible sets of four Cassegrain camera relays: the f/12.9 Wide-Field (WF) camera, and the f/30 Planetary Camera (PC). The CCD detectors are thinned, backside-illuminated, Texas Instruments 800 × 800 devices, with 15 μm pixels. The secondary obscurations in the WFPC relays are not in the telescope pupil plane and therefore vignette the beam in a field-dependent manner as illustrated in Figure 1. The presence of spherical aberration together with the variation of the pupil function causes field dependence on the PSF in the WFPC. Images of crowded star fields show that the obscuration is decentered typically by 5% at the center of the chip because of misalignments.

The Faint Object Camera (FOC) (Paresce 1990) is the only other SI with direct imaging capability. It is designed to sample the images at the highest resolutions that *HST* can deliver and operates primarily in the ultraviolet. The FOC consists of two main camera/detector combinations operating at f/48 and f/96. Each camera reimages the OTA focal plane 6′ off-axis and consists of an unobscured off-axis two-mirror Cassegrain, followed by filter wheels and a cylindrical fold lens which corrects the astigmatism from the OTA and allows focusing of the camera. The detectors are three-stage image intensifiers coupled by relay optics to an EBS TV tube. Apart from their filters, both cameras are all reflective and are therefore achromatic.

An indication of the spherical aberration in the *HST* optics came with the first light image in the WF camera. The image had a tight core containing ~10% of the light, a surrounding plateau containing most of the energy, and "tendrils" extending in apparently random directions from the plateau. Figure 2 (Plate L1) shows in detail one of the observed point-spread functions (PSF). The core comes from an inner zone of the primary mirror. The halo, which extends to a radius of 2″.0, comes from aberrated rays from the remainder of the pupil. The shadows of obscurations in the pupil (the primary mirror pads and the secondary spider supports) are clearly visible. Diffraction at these obscurations cause them to appear as "tendrils."

In Figure 3 (Plate L2), the left two columns show observed images of bright stars at two different scales, while the right columns show corresponding models. The top two rows show images taken on each side of the nominal focus position. These images clearly demonstrate the presence of spherical aberration. Instead of a uniformly illuminated pupil image, the inner or outer edges are brighter. Below the defocused images are a set taken at the nominal focal position with the WFPC and FOC through visible and ultraviolet filters. The third row contains the image from Figure 2. The Fraunhofer diffraction integral in the models is over the pupil function in Figure 1 and contains only spherical aberration and focus terms. The outer rings visible in the ultraviolet data (cases 4 and 6) caused by zonal mirror surface errors visible in the prelaunch mirror interferograms are not included in the models. There are also differences in detail in the cores of the images caused by pixel registration and attitude jitter. Otherwise, the agreement between the models and the data is excellent, which demonstrates that the aberration is simply characterized, and therefore may be optically corrected in future instruments. Table 1 presents data on cameras, filters, and focus positions shown in Figure 3. The focus setting is measured in microns at the secondary mirror, relative to an arbitrary conventional zero point. The Z_4 coefficient is the focus setting in waves rms at 547 nm used on the models. A change of 1 mm in the secondary mirror position corresponds to a change of 11.09 in Z_4.

TABLE 1

CAMERAS, FILTERS, AND FOCUS POSITIONS USED IN FIGURES 3, 4, AND 5

Case	Camera	Filter (nm)	Width (nm)	Date (1990)	Focus	Z_4 (waves)	Target
1.....	PC5	547	44	Jun 21	−312	−4.42	V = 12.3 near ι Car
2.....	PC5	547	44	Jun 23	+342	+2.70	V = 12.3 near ι Car
3.....	PC6	487	3.1	Aug 15	−10	−1.16	HD 124063
4.....	PC6	230	37	Aug 15	−10	−1.16	HD 124063
5.....	F96	486	3.4	Aug 15	−10	−1.16	GRW+705824
6.....	F96	120	8.6	Aug 15	−10	−1.16	GRW+705824

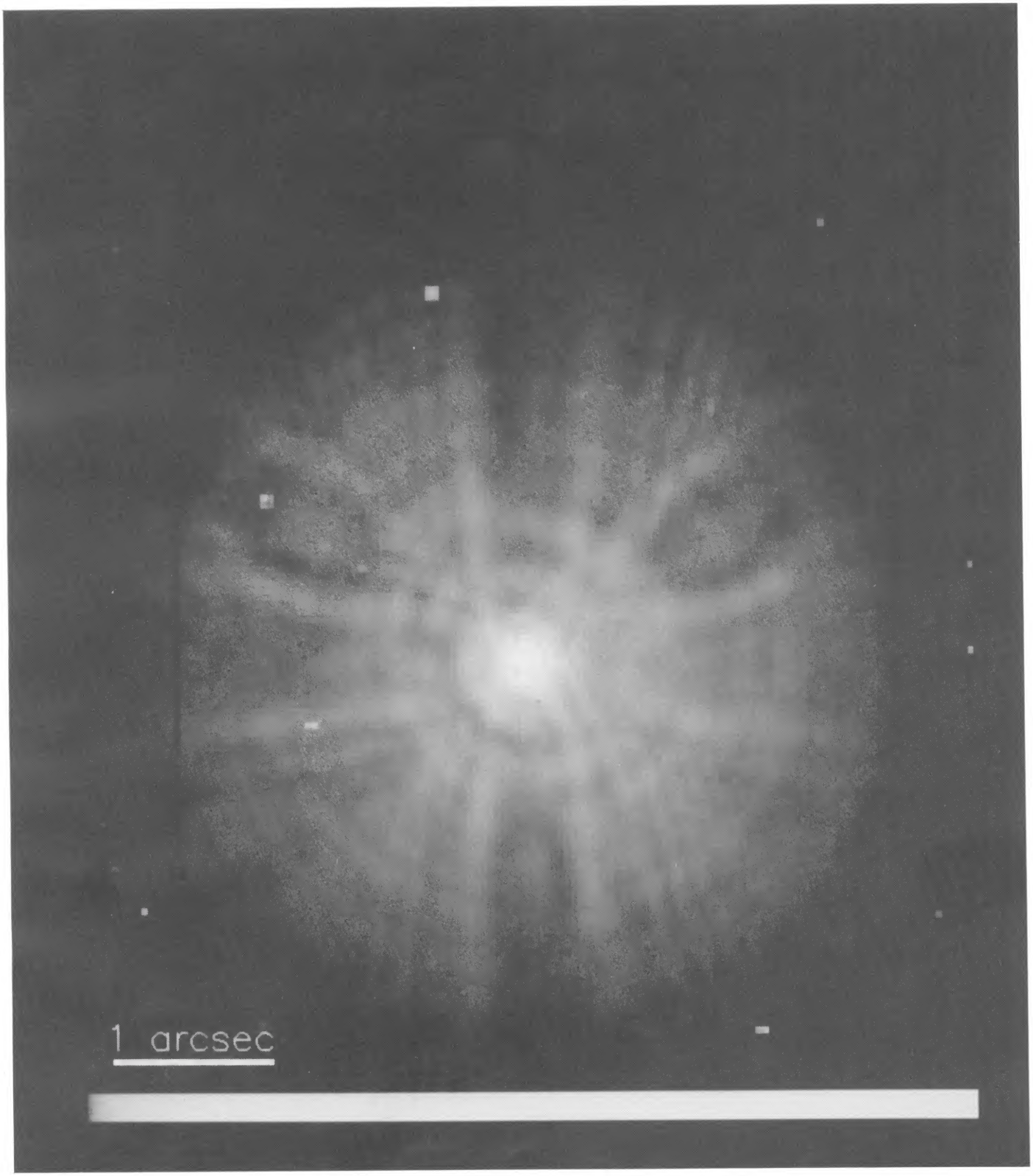

FIG. 2.—HD 124063 observed with the PC through a narrow filter centered at 487 nm at the focus setting used for the SAO/EROS observations

BURROWS et al. (see 369, L22)

PLATE L2

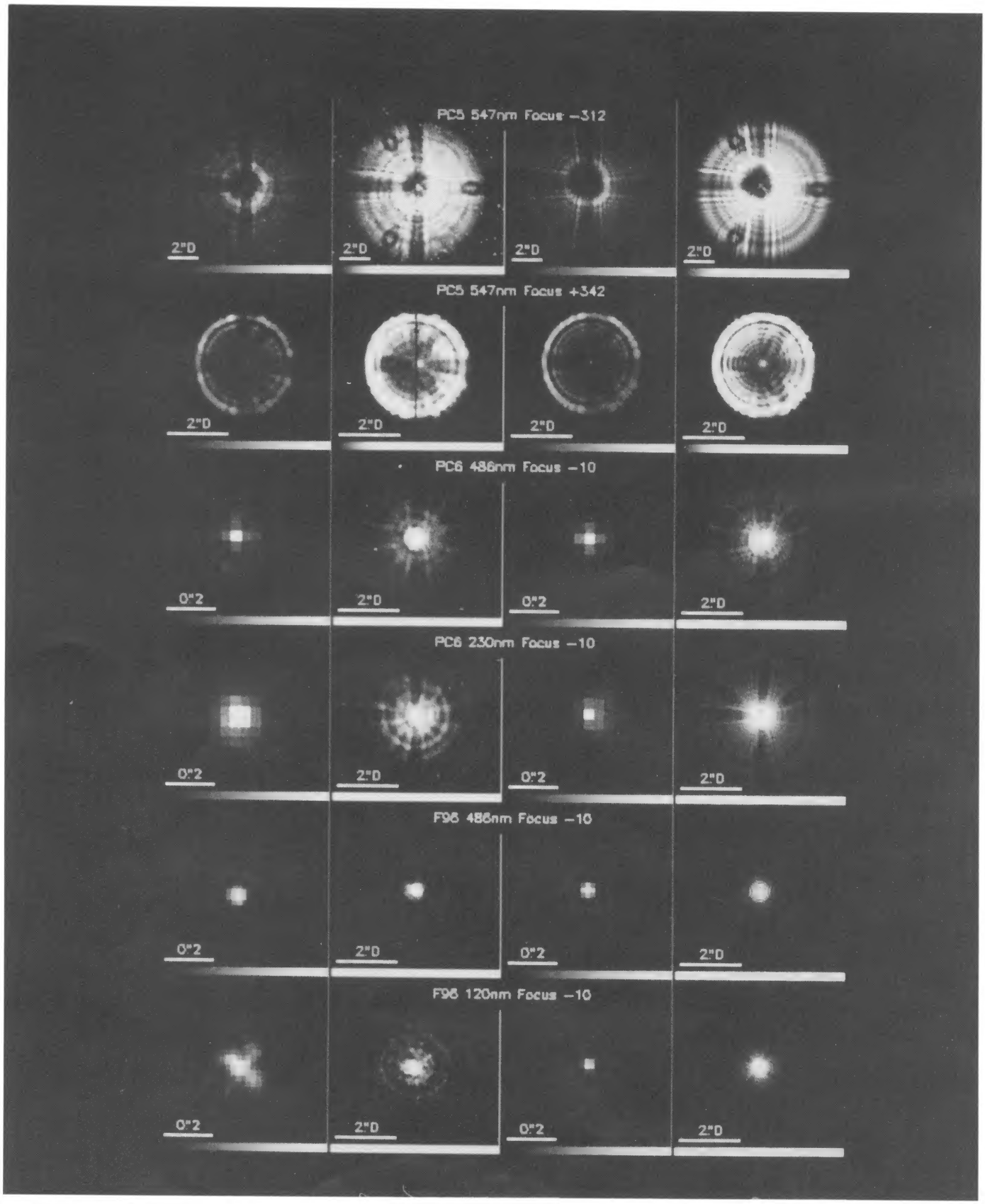

FIG. 3.—A montage showing, horizontally, the observed and predicted images of point sources in the presence of 0.43 waves (at 633 nm) of spherical aberration. The image core of the bottom four cases is magnified by a factor of 8 in order to bring out details. It is saturated in the unmagnified view, designed to show the profile of the image wings. The observed images are renormalized to an integral of unity, after subtracting a median filter estimate of the background level.

BURROWS et al. (see 369, L22)

The model fits to the camera images show that *HST* suffers from about −0.43 waves rms of spherical aberration at 633 nm. The error corresponds to a 4.6 μm optical path length error for marginal rays at the paraxial focus, a 1.″6 diameter circle of least confusion, a 2.3 μm surface error at the edge of the primary, or a change of the primary mirror conic constant from the specified −1.0022985 to about −1.014. The marginal focus is about 43 mm from the paraxial focus in the f/24 focal plane.

The spherical aberration is known to originate in the OTA because it affects images in the FOC as well as the WFPC as demonstrated by the bottom two rows of Figure 3. It is also affecting the wavefront sensors. The major error is on the primary mirror because of the absence of significant field coma.

A NASA commission (Allen et al. 1990) has uncovered an error of 1.31 mm in the placement of the field lens in the reflective null corrector used in the manufacture of the *HST* primary mirror. This error alone would lead to the primary mirror having a conic constant consistent with the value of −1.0133 that they derive from ground test interferograms and an on-axis wavefront error in the OTA of −0.40 waves rms at 633 nm, which is 7% less than the value reported here on the basis of on-orbit measurements.

Figures 4 and 5 show the observed azimuthally averaged PSFs and encircled energy for the four cases at nominal focus in Figure 3. The slightly lower encircled energy curves for the planetary camera compared to the FOC are due to a combination of the larger obscuration and additional vignetting caused by the internal misalignments at this field position and focus setting. Most of the energy is contained within the geometric image, but some will be scattered to still larger angles by mirror microroughness and diffraction on the *HST* pupil. Prelaunch predictions based on the primary mirror measurements (Schroeder 1987; Burrows 1990) indicate that about 5% of the light will be scattered to angles larger than 3.″0 at 633 nm, but this has not yet been measured. Instead, the encircled energy is defined here to be 100% at 3.″0 radius.

The on-axis image was expected to have wavefront aberrations totaling about 1/20 wave rms at 633 nm. The conventional definition of "diffraction-limited" is that the ratio of the peak of the PSF to the theoretical limit in the absence of aberrations (Strehl ratio) be greater than 0.8, corresponding to a wavefront error of better than 1/14 wave rms. By this definition, *HST* was expected to be diffraction-limited at visible wavelengths.

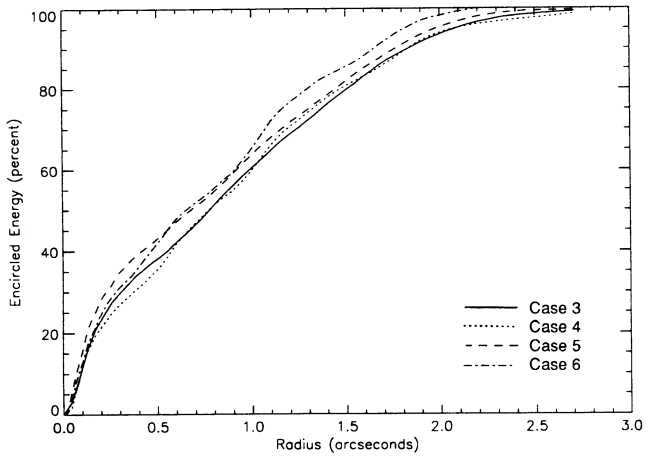

FIG. 4.—Encircled energy curves for FOC and PC images in the ultraviolet and visible (cases 3, 4, 5, and 6 in Table 1).

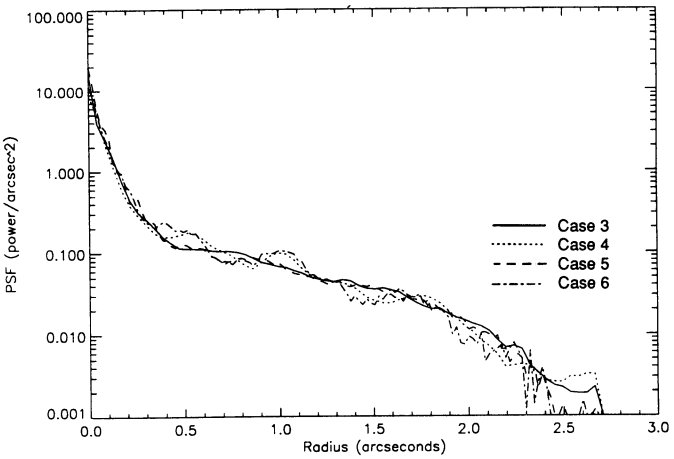

FIG. 5.—Log PSF curves for cases 3, 4, 5, and 6 in Table 1. The zonal errors that appear in the ultraviolet images are similar in both cameras.

A diffraction-limited telescope with the same central obscuration as *HST* would have 80% of the energy within 0.″1 radius at 633 nm which includes half of the second bright Airy ring. The *HST* specification was 70%, after allowing for diffraction on the other obscurations in the pupil, microroughness scattering, dust, and jitter. Instead, we obtain at best 16% at the nominal focus setting 13 mm from the paraxial focus. This focus position was selected for all the scientific observations reported in this issue and is close to the setting likely to be adopted for the General Observer program.

Our model calculations show that *HST* has a full width at half-maximum (FWHM) of 0.″078 instead of the expected 0.″052 at 633 nm. The FWHM is approximately proportional to wavelength in both cases. The encircled energy within a 0.″1 radius is 15.9% for the FOC and at best 11.8% for the WFPC. This difference is caused by the variable larger central obscuration in the WFPC. The Strehl ratio of *HST* was predicted to be 0.9 at 633 nm. It is 0.10 and decreases to 0.035 at 250 nm. For comparison, excellent ground-based astronomical seeing of 0.″5 FWHM through the same aperture telescope would give a Strehl ratio of 0.012 and encircled energy of 0.081 in 0.″1 radius.

3. POINTING PERFORMANCE

During observations, pointing information is provided by gyroscopes with periodic position updates supplied by two of the three FGS tracking guide stars. Control is obtained by varying the speed of reaction wheels. The FGSs have two operational modes: coarse track based on image centroiding, and fine lock based on an interferometric system. Fine lock was to have provided an image stability of 0.″007 rms. Coarse track was considered an intermediate step in the acquisition sequence and a degraded guiding mode (0.″021 rms for $V = 14.5$) for nondemanding observations.

The current performance of the guiding system is summarized in Figure 6. As indicated by the dotted line in the figure, coarse track has a variance inversely proportional to the count rate but equals the expected 0.″021 rms only for a 12th mag guide star. In fine lock, tracking is essentially within specifications during quiescent periods and is almost magnitude-independent. However, fine lock cannot be reliably obtained

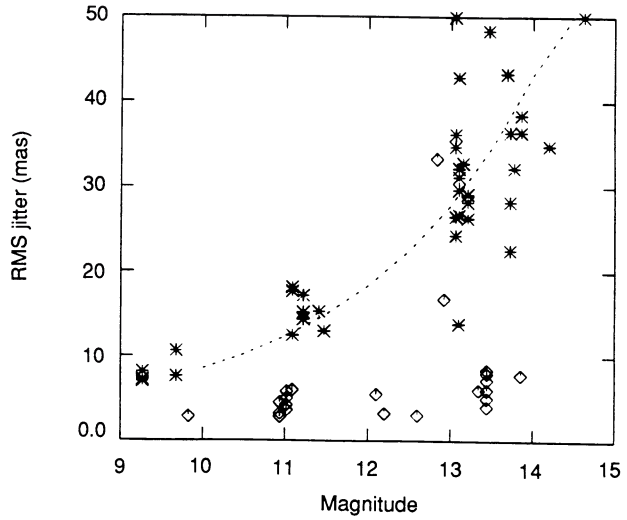

FIG. 6.—Tracking performance: rms pointing error in fine lock (*diamonds*) and coarse track (*stars*) as a function of stellar magnitude, during the most quiescent periods in the orbit. There are few points plotted in fine lock above $V = 13.5$ because the FGS generally loses lock on fainter stars. The dashed curve indicates that the coarse track pointing variance is inversely proportional to the number of detected photons.

with the full pupil, because of still imperfect alignment of the telescope, or secondary effects of the spherical aberration in the FGS optics. It is expected that tuning of system parameters will allow operation in fine lock at the predicted limit of 13.5 mag with the 2/3 aperture stop and will also improve coarse track.

The *HST* guiding system was designed to operate on stars of 14.5 mag to give an 85% probability of finding guide stars at high Galactic latitude. The effect of limiting the guide stars to 13.5 mag is more severe for the WFPC than for the other instruments, because rolling the spacecraft about an on-axis target does not add many new candidate guide stars. Sky coverage in fine lock for the WFPC is reduced to 70% for Galactic latitudes greater than 30° if only one pair of guide stars is needed or 25% if two pairs are required to avoid failures due to undetected binary stars.

Jitter and loss of lock is induced by day/night transitions. For 2–3 minutes associated with passage from orbital day to orbital night or vice versa, thermal shocks in the solar arrays create line of sight jitter with 150 mas peak-to-peak amplitude and components of 10 and 2 s periods. Smaller amplitude oscillations (0".015–0".050) occur intermittently during the remainder of the orbit. The points in Figure 6 exclude such disturbances. The day/night transitions almost always produce loss of fine lock, although coarse track with its larger dynamic range is maintained.

4. SCIENTIFIC IMPACT AND PROSPECTS

When the spherical aberration was discovered, it was decided to obtain realistic science observations to test the capabilities of the observatory. These data, called Science Assessment Observations (SAO), have so far been obtained for the two imaging cameras. The results, along with several Early-Release Observations (EROS) taken for public information purposes, are described in other *Letters* in this issue.

The SAO/EROS results are consistent with the above characterization of the PSF. Most of the imaging projects have dealt with high-surface-brightness objects such as Saturn, various galaxy nuclei, the core of a globular cluster, and several bright H II regions. Because of the sharp core and stability of the PSF, image deconvolution techniques can extract fine spatial detail from the original image. However, since deconvolution always amplifies noise, it is most successful on high-surface-brightness objects. Several *Letters* in this issue show deconvolved images that approach the image quality expected from *HST*.

Direct reference observations of the PSF for deconvolution purposes will usually suffer from different jitter to the target data. In any given image, the observed PSF is the convolution of the instantaneous PSF with a jitter blurring function. This function is observed by the FGS and gyros and can be determined from engineering telemetry. The use of model PSFs in conjunction with such data appears to be a promising approach, because the optics are simply characterized, and stable.

When there is substantial *a priori* information about the structure of the source, more can be done in image interpretation. The simplest example is a star field, where all the objects are known to be point sources. If the desired information is merely positions and approximate brightnesses, then the core of the PSF allows one to resolve binary stars at a separation close to the original power of the telescope. Several *Letters* use this ability including splitting the components of a gravitational lens, the massive star system R136a, and the Pluto-Charon system.

The shortcomings of the optics become painfully apparent when working on faint objects. Deconvolution on extended objects inevitably fails when the signal-to-noise ratio is low. For point sources, the limiting intensity is inversely proportional to the root mean square of the normalized PSF when background limited. At the SAO/EROS focus setting from the models, we compute a loss of 2.0 mag in limiting sensitivity for a given integration time. Stellar photometry tests show a loss of 2.5 mag on isolated stars and an even more significant loss on faint stars within the extended halo of brighter stars (Holtzman et al. 1990). It is clear that the loss of faint objects is a severe blow to the overall imaging capabilities, and the scientific program of the observatory.

Our understanding of the observatory performance is still at a preliminary stage in many respects. The optical problems are understood well enough to predict the effects on most observations, yet not quite well enough to prescribe corrective optics for future science instruments. The pointing system is fairly well characterized, but the effectiveness of flight software changes is still unclear. Finally, in areas such as sky background and baffling efficiency, UV throughput, target acquisition, internal optical alignments, and scattered light there are many unanswered questions. Most of these should be resolved by the end of the Science Verification (SV) period.

NASA plans to replace the WFPC with a "clone" instrument fitted with corrective optics. Provided that the prescription is determined adequately, the pointing control problems are overcome, and the internal alignments of the cameras with respect to the OTA can be improved over the present camera, we will substantially recover the expected scientific capabilities of the WFPC

This work was sponsored in part by NASA contract NAS5-26555.

REFERENCES

Allen, L., et al. 1990, The Hubble Space Telescope Optical Systems Failure Report (Washington: NASA)
Burrows, C. 1990, Optical Telescope Assembly Handbook (Baltimore: Space Telescope Science Institute)
Holtzman, J. A., et al. 1991, ApJ, 369, L35
Griffiths, R. 1990, Wide Field Planetary Camera Instrument Handbook (Baltimore: Space Telescope Institute)
Hall, D., ed. 1982, The Space Telescope Observatory (Washington: NASA Scientific and Technical Information Branch, 1)
Paresce, F. 1990, Faint Object Camera Instrument Handbook (Baltimore: Space Telescope Science Institute)
Schroeder, D. 1987, Astronomical Optics (Orlando: Academic Press)